

Exciton Stark shift and electroabsorption in monolayer transition-metal dichalcogenides

Thomas Garm Pedersen*

*Department of Physics and Nanotechnology, Aalborg University, DK-9220 Aalborg Øst, Denmark
and Center for Nanostructured Graphene (CNG), DK-9220 Aalborg Øst, Denmark*

(Received 14 June 2016; revised manuscript received 1 August 2016; published 16 September 2016)

Excitons in transition-metal dichalcogenides can be dynamically manipulated using electrostatic fields. Analyzing both in-plane and out-of-plane fields, I compute the exciton Stark shift and electroabsorption spectrum of monolayer MoS₂, MoSe₂, WS₂, and WSe₂. The effect of in-plane fields is found to greatly surpass that of out-of-plane fields. In particular, if exciton binding is reduced through screening by surrounding dielectrics, such as in MoS₂ encapsulated by hexagonal boron-nitride, the in-plane exciton polarizability exceeds the measured out-of-plane value by nearly two orders of magnitude. Accordingly, pronounced electroabsorption features are expected for fields as low as 10 V μm⁻¹.

DOI: [10.1103/PhysRevB.94.125424](https://doi.org/10.1103/PhysRevB.94.125424)**I. INTRODUCTION**

The interest in transition-metal dichalcogenides (TMDs) has recently increased dramatically. These materials have intriguing electronic and optical properties and serve as versatile building blocks in van der Waals stacked devices [1–2]. The linear and nonlinear optical properties of semiconducting TMDs are dominated by excitons [1–6]. In monolayer structures with little substrate screening, the exciton binding energy is as large as 0.5 eV [3–6]. Hence, such electron-hole pairs are stable against thermal dissociation. This has significant implications for optoelectronic devices, and excitons play a crucial role in TMD photodetectors [7,8] and light emitting diodes [9]. The properties of excitons in TMDs can be controlled by structural manipulation as well as gating. Hence, increased screening in multilayer structures due to ambient dielectrics will reduce exciton binding. It is highly desirable, however, to find means of manipulating excitons that can be switched on and off at will. Such *dynamical* control is possible using external gating via applied electric fields. Hence, in several recent works, tunability through gating was demonstrated for exciton photoluminescence, electroluminescence, and second harmonic generation [9–14]. The dominant mechanism in many cases is electrically controlled doping that affects screening and changes the balance between neutral and charged excitons (trions) [10,13,14].

Very recently, a purely electrostatic Stark shift of the exciton emission was observed [15], thus demonstrating that tuning of the emission without doping is possible. This demonstration was achieved in vertically biased MoS₂ few-layer samples. Hence, detection of the Stark shift was made possible by the very large fields (of order 100 V μm⁻¹) that can be applied perpendicularly to such very thin samples. The measured out-of-plane polarizability was found to be $\beta_{\perp} = \frac{1}{2}\alpha_{\perp} \approx 0.58 \times 10^{-8} \text{ Dm V}^{-1} = 1.2 \times 10^{-19} \text{ eV(m/V)}^2$. Hence, a field of $\mathcal{E} = 100 \text{ V } \mu\text{m}^{-1}$ produces a noticeable Stark shift of $-\frac{1}{2}\alpha_{\perp}\mathcal{E}^2 \approx -1.2 \text{ meV}$. (Note that the standard notation is followed and that α rather than β is defined as the polarizability below. The two definitions are related by $\beta = \frac{1}{2}\alpha$.) It is clear, however, that much greater

Stark shifts are, in principle, possible using in-plane electric fields, as the in-plane exciton polarizability is much greater than the out-of-plane value. In practice, exploiting in-plane Stark shifts could obviously be challenging because of the need for electrodes closely spaced laterally. Provided such practical difficulties can be overcome, however, the large polarizability could pave the way for greater tunability with smaller applied fields. Recently, optical Stark shifts in TMDs due to in-plane polarized electromagnetic fields have been observed [16,17].

In the present paper, in-plane fields are primarily considered, and the exciton Stark shift and electroabsorption of several important TMDs—MoS₂, MoSe₂, WS₂, and WSe₂—are studied. Very large Stark shifts and pronounced electroabsorption features are predicted. Thus, for MoS₂ encapsulated by hexagonal boron-nitride (hBN), an in-plane polarizability that is nearly two orders of magnitude larger than the experimental out-of-plane value and six orders of magnitude larger than that of an unscreened two-dimensional (2D) hydrogen atom is found. Hence, electric fields of the order 10 V μm⁻¹ are expected to lead to substantial Stark shifts. The 2D Wannier model [18,19], including a strong in-plane electrostatic field similar to recent studies of Stark shifts in phosphorene [20] and exciton ionization in TMDs [21,22], is applied. In this manner, general results for the screening-dependent polarizability are found. In addition, the electroabsorption spectrum of important TMDs is computed, and significant spectral changes for fields around 10 V μm⁻¹ are predicted. Finally, the differences between in-plane and out-of-plane fields are analyzed by constructing a simple quantum well model of the out-of-plane case.

II. EXCITON STARK SHIFT

The TMD excitons are modeled as electron-hole pairs whose interaction is screened by the TMD sheet itself as well as surrounding dielectrics. In the two-band, effective mass approximation, such excitons are described by the 2D Wannier equation [18,19]. This equation resembles that of a 2D hydrogen atom except that in-plane (\parallel) effective masses $m_{e,\parallel}$ and $m_{h,\parallel}$ enter the kinetic energy of electrons and holes, respectively. Moreover, screening modifies the Coulomb interaction. Atomic units (a.u.) are used measuring distances in atomic Bohr radii a_B and energies in atomic Hartrees Ha

*tgp@nano.aau.dk

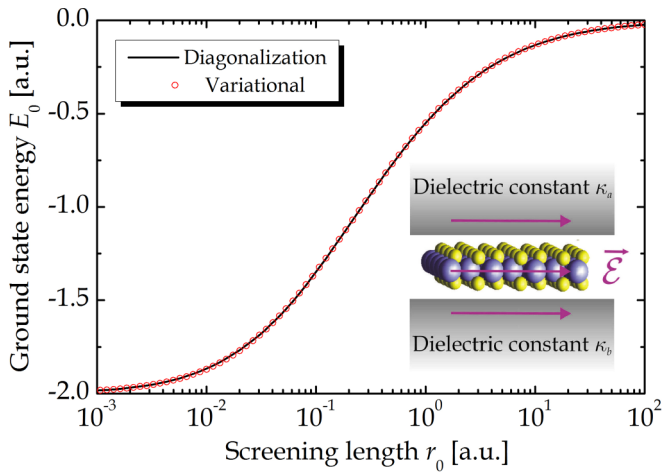


FIG. 1. Energy of the exciton ground state using numerical diagonalization and a variational approach. The inset illustrates the geometry of the TMD sample.

and an in-plane electrostatic field $\vec{\mathcal{E}}$ is included. In terms of the relative coordinate $\vec{r} = \vec{r}_e - \vec{r}_h$ of the electron-hole pair, the Wannier equation reads

$$\left\{ -\frac{1}{2\mu} \nabla^2 - w(\vec{r}) + \vec{\mathcal{E}} \cdot \vec{r} \right\} \psi(\vec{r}) = E \psi(\vec{r}). \quad (1)$$

Here, $\mu = m_{e,\parallel} m_{h,\parallel} / (m_{e,\parallel} + m_{h,\parallel})$ is the reduced in-plane exciton mass in units of the free-electron mass. The potential w is the screened Coulomb attraction. In truly 2D semiconductors, such as monolayer TMDs, screening is nonlocal, i.e., it displays a pronounced q dependence in momentum space [23,24]. To capture this effect, the dielectric constant $\varepsilon(\vec{q})$ can be approximated by the linearized function $\varepsilon(\vec{q}) \approx \kappa + r_0 q$. Here, $\kappa = (\kappa_a + \kappa_b)/2$ is the average of the dielectric constants of the surrounding materials above and beneath the sheet, as illustrated in the inset of Fig. 1. In addition, r_0 is the screening length proportional to the sheet polarizability [24]. In real space, this interaction is given by the Keldysh [23] form

$$w(r) = \frac{\pi}{2r_0} \left[H_0\left(\frac{\kappa r}{r_0}\right) - Y_0\left(\frac{\kappa r}{r_0}\right) \right]. \quad (2)$$

Here, H_0 is the zeroth order Struve function, and Y_0 is the zeroth order Bessel function of the second kind, respectively. This potential has an unscreened r^{-1} behavior at large distances but diverges only logarithmically at small distances due to screening.

In the presence of an in-plane electrostatic field, the excitonic states become unstable, and the eigenvalue E attains a nonvanishing imaginary part corresponding to the ionization rate [21,22,25]. The real part of E is shifted by the field, and the lowest order becomes $E \approx E_0 - \frac{1}{2}\alpha \mathcal{E}^2$, where E_0 is the unperturbed energy and α is the exciton polarizability. The Wannier problem contains three material parameters, μ , κ , and r_0 , upon which the energy will depend. However, a simple scaling analysis readily shows that

$$\begin{aligned} E_0(\mu, \kappa, r_0) &= \frac{\mu}{\kappa^2} E_0(1, 1, \tilde{r}_0), \\ \alpha(\mu, \kappa, r_0) &= \frac{\kappa^4}{\mu^3} \alpha(1, 1, \tilde{r}_0), \end{aligned} \quad (3)$$

where $\tilde{r}_0 = (\mu/\kappa^2)r_0$ is the effective screening length. Hence, only the dependence on \tilde{r}_0 is nontrivial. In the following, the analysis is therefore restricted to the simplified problem,

$$\left\{ -\frac{1}{2} \nabla^2 - \frac{\pi}{2r_0} \left[H_0\left(\frac{r}{r_0}\right) - Y_0\left(\frac{r}{r_0}\right) \right] + \vec{\mathcal{E}} \cdot \vec{r} \right\} \psi(\vec{r}) = E \psi(\vec{r}), \quad (4)$$

where $\mu = \kappa = 1$ and the scaling relations [Eq. (3)] are used to generalize to arbitrary situations. Note that μr_0 is in the range 10–30 a.u. for typical TMDs [4].

The perturbative regime, in which the energy depends quadratically on the field and exciton ionization is negligible, is restricted to low field strengths. In atomic problems, the critical field strength is given by 1 a.u., i.e., $\mathcal{E}_0 = \text{Ha}/ea_B = 5.14 \times 10^{11} \text{ V m}^{-1}$. As an estimate for solid-state problems, the effective Hartree $\text{Ha}^* = \text{Ha} \times \mu/\kappa^2$ and Bohr radius $a_B^* = a_B \times \kappa/\mu$ can be assumed, and a critical field of $\mathcal{E}_0^* = \mathcal{E}_0 \times \mu^2/\kappa^3$ can then be found. Adopting $\mu \approx 0.2$ and $\kappa \approx 5$ as typical parameters for in-plane fields, it follows that the perturbative regime is restricted to fields well below $\mathcal{E}_0^* \approx 165 \text{ V } \mu\text{m}^{-1}$. This is in agreement with Ref. [21], for which a marked deviation from the quadratic field dependence is noted around this field strength for MoS₂ encapsulated in hBN sheets.

The unperturbed problem, i.e., Eq. (4) with $\mathcal{E} = 0$, has cylindrical symmetry, and the ground state is of the purely radial form $\psi_0(r)$. In the presence of the field, polar coordinates are applied, such that $\vec{\mathcal{E}} \cdot \vec{r} = \mathcal{E} r \cos \theta$. It is then easily demonstrated that the exact first order correction to the wave function is of the form $\psi_1(r) \cos \theta$ with, additionally, $\psi_1(0) = 0$. The Wannier problem [Eq. (4)] for the ground state exciton is solved by using two approaches: (1) diagonalization in a Gaussian basis and (2) variational optimization. As shown below, these approaches yield excellent agreement for both energy and polarizability. In the calculation of the unperturbed ground state, the Gaussian basis contains 15 members of the form $\exp(-\beta_i r^2)$ with $\beta_i = 10^{-3} \times 3^i$, $i = 0 \dots 14$. To additionally include the first order correction $\psi_1(r) \cos \theta$, functions of the form $r \cos \theta \exp(-\beta_i r^2)$ with the same set of exponents are added.

The exciton polarizability can be obtained in several distinct ways. By ensuring that these agree, the reliability of the results can be assured. The conceptually simplest approach is to diagonalize the Wannier problem, including the electrostatic field. This finite-field approach is well known from atomic and molecular polarizability calculations [26] and has been applied to phosphorene [20] and MoS₂ [21]. The danger of the finite-field approach is that the applied field strength must be sufficiently high that numerical errors are suppressed. This, however, means that care must be taken that higher-order contributions to the energy are negligible. In practice, a field of $\mathcal{E} = 10^{-4}$ a.u. is found to be appropriate.

As an alternative to the finite-field approach, the starting point for the variational approach is finding an accurate ansatz for the unperturbed ground state. Subsequently, this zeroth order solution can be used to find an accurate first order correction to the wave function. In the Dalgarno-Lewis [27] method, this yields the exact polarizability provided that the exact unperturbed state is used as input. It is important to

note that only the first order correction to the wave function is needed to find the second order correction to the energy [27]. Alternatively, the first order wave function can be formulated in a variational form itself. Below, both approaches are followed and shown to agree rather well with each other as well as the finite-field approach. A flexible bi-exponential form is used as a variational ansatz for the unperturbed ground state,

$$\psi_0(r) = N\{e^{-ar} - be^{-\gamma ar}\}, \quad (5)$$

where N is a normalization constant, whereas a , b , and γ are variationally optimized. The comparison in Fig. 1 shows that this ansatz is able to reproduce the exact solution to a very high degree of accuracy over the entire range of screening lengths. Moreover, the values in Fig. 1 agree with those of Ref. [28] to within four digits.

Writing $\psi_1(r) = -2\mathcal{E}\psi_0(r)f(r)$, the exact wave function to first order in the electric field can be written in the form

$$\psi(\vec{r}) = \psi_0(r)[1 - 2\mathcal{E}f(r)\cos\theta]. \quad (6)$$

The factor $2\mathcal{E}$ is pulled out to simplify notation below. Provided ψ_0 is the exact zero order solution, the expression [Eq. (6)] leads to the second order energy

$$E_2 = \mathcal{E}^2\langle\psi_0|[f'(r)]^2 + [f(r)/r]^2 - 2rf(r)|\psi_0\rangle, \quad (7)$$

with primes indicating radial derivatives. Note that this result is based on a vanishing first order correction to the energy as ensured by the cylindrical symmetry of the unperturbed problem. Next, two approaches can be followed: In the Dalgarno-Lewis [27] approach, functional minimization is applied to Eq. (7). In this manner, the optimal f obeys

$$-f''(r) - \left(2\frac{\psi_0'}{\psi_0} + \frac{1}{r}\right)f'(r) + \frac{1}{r^2}f(r) - r = 0. \quad (8)$$

Alternatively, a trial form may be used and optimized in Eq. (7). To this end, the form $f(r) = pr(1 + qr)$ with p and q variational parameters has been adopted. It should be emphasized that both Eqs. (7) and (8) assume ψ_0 to be the exact unperturbed ground state. Since no exact analytical solution is known, the ground state obtained from numerical diagonalization or the variational ansatz [Eq. (5)] is used for approximation.

Figure 2 compares the computed exciton polarizability using three separate approaches: (1) the finite-field method, (2) the variational optimization of the first order wave function, and (3) the Dalgarno-Lewis approach based on solving Eq. (8) numerically. As evident from the figure, all three approaches agree rather well. Moreover, the exact result $\alpha = 21/128$ [25,29] is reproduced in the unscreened limit $r_0 \rightarrow 0$ corresponding to a 2D hydrogen atom. This agreement testifies to the quality of the variational ansatz Eq. (5). Note, also, that the limit as r_0 exceeds unity is well approximated by the power-function fit $\alpha \approx 3.5r_0^{1.8}$. This means that polarizabilities far larger than the 2D hydrogen atom result can be expected for $r_0 \gg 1$. In fact, for realistic values of r_0 in TMDs, polarizabilities at least three orders of magnitude larger than the unscreened value are found. Moreover, if additional screening by the surrounding dielectrics is added, even larger values result.

To extract quantitative polarizabilities for specific materials, the normalized a.u. results above are now converted,

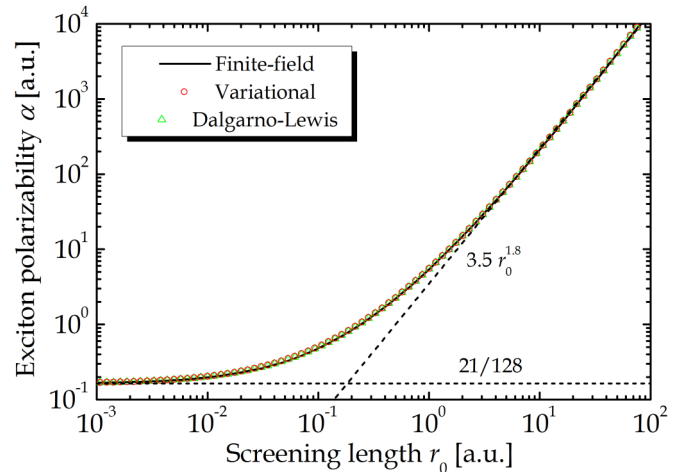


FIG. 2. Comparison of the exciton polarizability using different computational approaches. The horizontal dashed line is the result for the 2D hydrogen atom, and the inclined dashed line is a power-function fit.

recalling that the a.u. of polarizability is $e^2 a_B^2 / \text{Ha} = 1.03 \times 10^{-22} \text{eV}(\text{m/V})^2$. To this end, the generic values in Fig. 2 are combined with the scaling Eq. (3) using *ab initio* values for μ and r_0 from Ref. [4]. For four important materials, this yields the following: $\tilde{r}_0(\text{MoS}_2) = 23.45/\kappa^2$, $\tilde{r}_0(\text{MoSe}_2) = 26.13/\kappa^2$, $\tilde{r}_0(\text{WS}_2) = 16.59/\kappa^2$, and $\tilde{r}_0(\text{WSe}_2) = 20.09/\kappa^2$. When plotted against the substrate screening κ , the converted exciton polarizability and binding energy are as shown in Fig. 3. The unscreened ($\kappa = 1$) exciton binding energy is around 0.5 eV for all four materials, in agreement with previous results [4]. This is reduced by nearly an order of magnitude, as the substrate screening is increased tenfold. Importantly, the polarizability increases by an order of magnitude with increased screening. Hence, at $\kappa = 10$ the polarizability reaches values in the range of $\alpha = 45 \times 10^{-18} \text{eV}(\text{m/V})^2$ to $70 \times 10^{-18} \text{eV}(\text{m/V})^2$. Focusing on freely suspended ($\kappa = 1$) MoS₂ and WSe₂, the polarizabilities are $\alpha = 4.6 \times 10^{-18} \text{eV}(\text{m/V})^2$ and $\alpha = 6.3 \times 10^{-18} \text{eV}(\text{m/V})^2$,

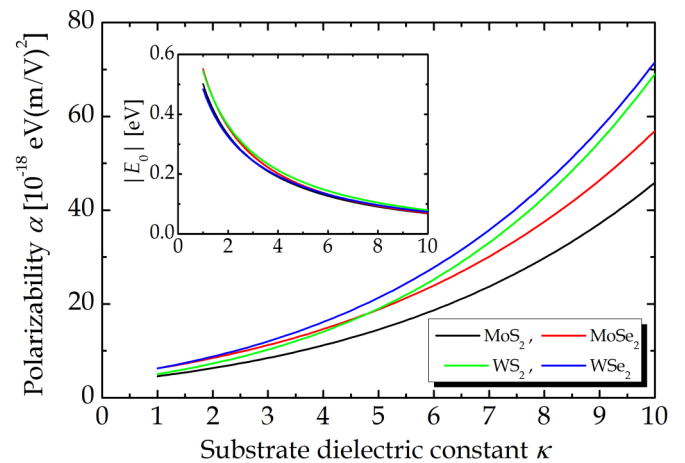


FIG. 3. Converted results for various TMDs. The main panel and inset show the converted exciton polarizability and binding energy versus substrate screening, respectively.

respectively. However, by encapsulating the same materials in hBN ($\kappa = 4.9$ [30]), the polarizabilities become $\alpha = 14.2 \times 10^{-18} \text{ eV(m/V)}^2$ and $\alpha = 20.8 \times 10^{-18} \text{ eV(m/V)}^2$, respectively. For MoS₂, this value is nearly two orders of magnitude larger than the out-of-plane value [15]. Note that the ground state exciton Stark shift for the x direction of phosphorene on SiO₂ ($\kappa = 2.4$) computed in Ref. [20] corresponds to a polarizability of $7.4 \times 10^{-18} \text{ eV(m/V)}^2$. Hence, this value agrees very well with the range predicted here. In addition, the effective dielectric constant results of Ref. [21] are $\alpha = 3.1 \times 10^{-18} \text{ eV(m/V)}^2$ for suspended MoS₂ and $\alpha = 6.1 \times 10^{-18} \text{ eV(m/V)}^2$ for MoS₂ encapsulated by single hBN sheets (in contrast to bulk hBN used here). These values also agree reasonably with the present results.

III. EXCITON ELECTROABSORPTION

The effects of electrostatic fields on the absorptive properties of TMDs are now discussed. This constitutes the exciton Franz-Keldysh effect that has previously been investigated for one-dimensional [31], two-dimensional [19], and three-dimensional semiconductors [32]. In the absence of excitonic effects, the Franz-Keldysh effect manifests itself in field-induced absorption below the band gap and characteristic oscillations in the absorption spectrum above the gap [33]. The presence of bound excitons alters the spectral features in a qualitative manner. Primarily, the Stark shift of the bound states leads to a red-shift of absorption peaks in contrast to the field-induced above-gap oscillations, which blue-shift with increased electric field.

Computing the entire spectrum, including bound as well as ionized states, is obviously more challenging than finding just the exciton ground state. Assuming k -independent momentum matrix elements, the exciton oscillator strength is determined by the exciton wave function evaluated at the origin [34]. In turn, the exciton susceptibility is given by the expression

$$\chi(\omega) = \chi_0 \sum_{\text{exc}} \frac{|\psi_{\text{exc}}(0)|^2}{E_{\text{exc}} [E_{\text{exc}}^2 - (\hbar\omega + i\hbar\Gamma)^2]}, \quad (9)$$

where χ_0 is a material dependent constant. Also, the sum is over all (bound and ionized) exciton states, with wave function $\psi_{\text{exc}}(\vec{r})$ and energy E_{exc} relative to the ground state. Finally, $\hbar\Gamma$ is a phenomenological line shape broadening. In the absence of the electrostatic perturbation, cylindrical symmetry implies eigenstates of the form $\psi_{mn}(\vec{r}) = R_n(r) \exp(im\theta)$ with m integer. Hence, the fact that the spectral response is proportional to $|\psi_{\text{exc}}(0)|^2$ means that only s -type states having $m = 0$ contribute. The presence of the electric field mixes states of different angular momentum m . To obtain an accurate representation of the actual eigenstates, a large basis covering a sufficient range of angular momenta is needed. Also, the basis must contain elements sufficiently delocalized to describe ionized states. One natural choice is a Bessel function basis $\psi_{mn}(\vec{r}) = J_m(\lambda_{mn}r/R) \cos(m\theta)$, where J_m is the m th Bessel function of the first kind and λ_{mn} is its n th zero, i.e., $J_m(\lambda_{mn}) = 0$. This approach effectively corresponds to introducing an infinite potential wall at $r = R$. However, if R is sufficiently large, the effect of this artificial confinement is negligible. Note that $\cos(m\theta)$ rather than $\exp(im\theta)$ is used

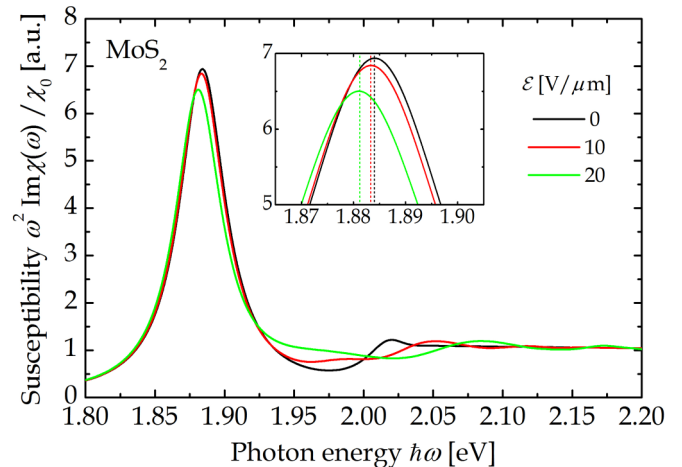


FIG. 4. Electroabsorption spectra of MoS₂ encapsulated by hBN. The black curve is the unperturbed case. The inset is a zoom of the exciton resonance with the vertical dashed lines indicating the predicted Stark shifts.

as appropriate for a perturbation varying as $\cos\theta$. For the spectra below, a basis of seven different angular momenta ($m = 0, \dots, 6$) and 400 states for each value of m has been used. The radial potential wall is taken at $R = \mu^{-1} \cdot 500$ a.u. and $\hbar\Gamma = 20$ meV.

The Franz-Keldysh spectra of MoS₂ and WSe₂ encapsulated in hBN are shown in Figs. 4 and 5, respectively. In these spectra, only the A exciton is included. To simulate more realistic spectra, the B exciton should be added as a roughly identical spectrum displaced in energy by the spin-orbit splitting. Also, the band gap has been adjusted such that the A exciton coincides with the experimental resonance. An important feature of these spectra is the observable Stark shift of the fundamental exciton. The vertical lines in both figures are the predicted Stark shifts based on the polarizability discussed in the previous section. It is seen that these predictions are in excellent agreement with the red-shifts found in the numerical electroabsorption spectra. In addition, the peak height decreases with field strength. This is natural considering the fact that the field tends to separate electrons

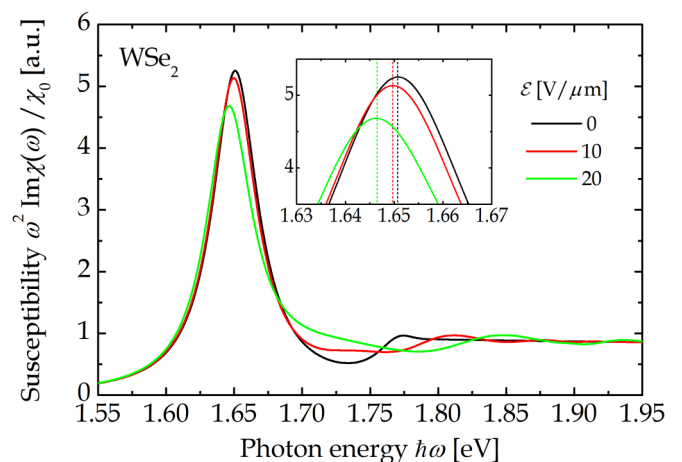


FIG. 5. Same as Fig. 4 but for WSe₂ encapsulated by hBN.

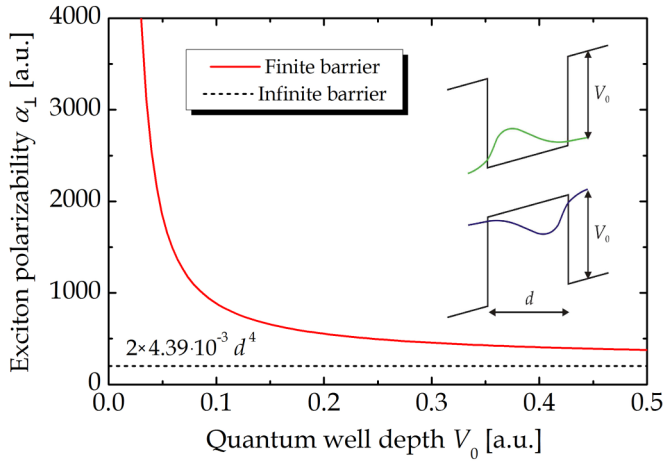


FIG. 6. Out-of-plane polarizability versus potential barrier. The full and dashed lines show finite and infinite barrier results, respectively. The model and parameters are defined in the inset, illustrating the tilted quantum well with polarized electron (green) and hole (blue) states.

and holes and, thereby, decreases the oscillator strength $|\psi_{\text{exc}}(0)|^2$ [35]. The characteristic field-induced oscillations in the above-gap spectrum are clearly visible for both MoS₂ and WSe₂. Moreover, the period of the oscillations increases with field (roughly as $\mathcal{E}^{2/3}$) as anticipated [33]. The red-shift of the bound exciton is expected to show in luminescence as well as absorption. In addition, the field-induced oscillations are expected to be visible in various types of spectroscopy, including electroabsorption and electroreflection. The fact that such pronounced features are predicted for moderate field strengths of the order $10 \text{ V}\mu\text{m}^{-1}$ means that future experimental observations are certainly realistic.

IV. OUT-OF-PLANE POLARIZABILITY

As the pioneering experiments in Ref. [15] were concerned with the out-of-plane polarizability, the crucial differences with respect to the in-plane case considered above are now discussed. Nearly identical Stark shifts were measured in MoS₂ samples consisting of one to five monolayers. However, the applied photoluminescence detection technique presumably is only sensitive to excitons, for which electrons and holes are located in the same monolayer. Thus, the experiment effectively probes individual monolayers. Electron-hole pairs in a TMD monolayer of thickness $d \sim 6.5 \text{ \AA}$ are relatively insensitive to perpendicular electric fields due to the tight confinement in the out-of-plane direction. Moreover, such tight confinement means that the electron-hole Coulomb attraction has little influence on the carrier motion in this direction. Ignoring atomistic details, the out-of-plane case can be modelled as a square well for both electrons and holes, as illustrated in the inset of Fig. 6. Here, for simplicity, identical barrier heights V_0 are assumed for both carriers. The polarizability of a single particle of mass m in an *infinite-barrier* quantum well is $(15 - \pi^2)/(12\pi^4) \cdot md^4$ a.u. [36,37]. Ignoring Coulomb effects, the exciton polarizability is obtained by summing electron and hole contributions, i.e., $\alpha_{\perp}^{(\infty)} = (15 - \pi^2)/(12\pi^4) \cdot Md^4$ a.u., where $M = m_{e,\perp} + m_{h,\perp}$ is the total mass comprised of the

effective masses for the out-of-plane direction (\perp). In the supplementary information of Ref. [15], the polarizability was incorrectly stated as $\alpha_{\perp}^{(\infty)} = \mu d^4$ a.u., i.e., without the prefactor $(15 - \pi^2)/(12\pi^4) \approx 4.39 \times 10^{-3}$ and using the in-plane reduced mass rather than the out-of-plane total mass. This led to the conclusion that the infinite barrier model was in good agreement with experiments. However, even if free-electron masses are used for out-of-plane effective masses so that $M = 2$, the correct expression $\alpha_{\perp}^{(\infty)} \approx 2 \times 4.39 \times 10^{-3} d^4$ a.u. ≈ 200 a.u. $\approx 2 \times 10^{-20} \text{ eV}(\text{m/V})^2$ is more than an order of magnitude below the experimental value $\alpha_{\perp} \approx 2.4 \times 10^{-19} \text{ eV}(\text{m/V})^2$ [15].

Since Coulomb effects will serve only to reduce the theoretical estimate, the reason for the discrepancy between calculation and experiment must be sought elsewhere. The most likely candidate is the unjustified assumption of infinite-barrier confinement. In reality, finite barriers of the order $V_0 \sim 0.1$ a.u. should be applied. The leakage of wave functions into the barriers leads to an increase in polarizability. To accurately model this effect, a quantum well with finite barriers is considered, and, again, the Dalgarno-Lewis [28] technique is applied, similar to the treatment in Ref. [37]. Briefly, starting from the exact unperturbed single-particle wave function $\psi_0(x)$, one writes the perturbed one as $\psi(x) = \psi_0(x)[1 - \mathcal{E}f(x)]$. Solving the first order problem immediately provides the derivative of f as $f'(x) = 2\psi_0^{-2}(x) \int_{-\infty}^x \psi_0^2(x')x'dx'$. Finally, the polarizability is simply $\alpha_{\perp} = M \int_{-\infty}^{\infty} [\psi_0(x)f'(x)]^2 dx$. This method is ideally suited to the present problem as the exact unperturbed wave function is known once a simple nonlinear algebraic equation for the energy is solved numerically [37].

In Fig. 6, the barrier dependence of the out-of-plane polarizability is shown assuming $M = 2$ and $d = 6.5 \text{ \AA} = 12.3$ a.u.. It is seen that quite a dramatic increase is found compared to the infinite barrier limit. Thus, for $V_0 = 0.1$ a.u., the polarizability increases by a factor of 4.4 relative to the infinite barrier value. In the experiments [15], MoS₂ was sandwiched between SiO₂ and Al₂O₃ barriers. The relevant band offsets have been measured in Ref. [38]. Hence, for the conduction band offset, one finds 3.01 eV and 3.56 eV for MoS₂/SiO₂ and MoS₂/Al₂O₃, respectively, while the corresponding numbers for the valence band are 4.19 eV and 3.31 eV. Using the average of these values as an estimate, it is found that $V_0 \approx 3.5 \text{ eV} = 0.128$ a.u. corresponding to an increase by a factor 3.7 relative to the infinite barrier. This calculated value is still significantly smaller than the experiment. However, a match with the experimental value can be achieved if a slightly increased quantum well thickness of $d = 9.8 \text{ \AA}$ is assumed. Hence, given the simplistic model (square barriers, free-electron masses, no atomistic detail, etc.) as well as uncertainties in the measured result, the agreement with experiments is reasonable.

V. SUMMARY

In summary, the possibilities of manipulating excitons in monolayer TMDs through in-plane electrostatic fields have been explored. Excitons are described using a 2D Wannier model incorporating the electric field and states are found through a combination of diagonalization and variational

approaches. The sensitivity to in-plane fields is predicted to be much greater than the known effects of out-of-plane fields. Including the influence of screening by surrounding dielectrics, a further increase in sensitivity is found. Hence, for MoS₂ encapsulated by hBN, the in-plane exciton polarizability is nearly two orders of magnitude larger than the measured out-of-plane value. The associated electroabsorption spectrum displays a red-shift of bound excitons and characteristic field-induced oscillatory spectral features above the band gap. Clearly observable features that appear at field strengths around 10 V μm⁻¹ are predicted. Finally, the out-of-plane

polarizability has been discussed in terms of a square well model for the perpendicular confinement.

ACKNOWLEDGMENTS

This paper is financially supported by the Center for Nanostructured Graphene (CNG) and the QUSCOPE center. CNG is sponsored by the Danish National Research Foundation, Project No. DNRFF103, and QUSCOPE is sponsored by the Villum Foundation.

-
- [1] Q. H. Wang, K. Kalantar-Zadeh, A. Kis, J. N. Coleman, and M. S. Strano, *Nature Nanotech.* **7**, 699 (2012).
- [2] A. K. Geim and I. V. Grigorieva, *Nature* **499**, 419 (2013).
- [3] A. Ramasubramaniam, *Phys. Rev. B.* **86**, 115409 (2012).
- [4] T. Olsen, S. Latini, F. Rasmussen, and K. S. Thygesen, *Phys. Rev. Lett.* **116**, 056401 (2016).
- [5] D.Y. Qiu, F. H. da Jornada, and S. G. Louie, *Phys. Rev. Lett.* **111**, 216805 (2013).
- [6] M. L. Trolle, G. Seifert, and T. G. Pedersen, *Phys. Rev. B.* **89**, 235410 (2014).
- [7] O. Lopez-Sanchez, D. Lembke, M. Kayci, A. Radenovic, and A. Kis, *Nature Nanotech.* **8**, 497 (2013).
- [8] M. Massicotte, P. Schmidt, F. Violla, K. G. Schädler, A. Reserbat-Plantey, K. Watanabe, T. Taniguchi, K. J. Tielrooij, and F. H. L. Koppens, *Nature Nanotech.* **11**, 42 (2016).
- [9] F. Withers, O. Del Pozo-Zamudio, A. Mishchenko, A. P. Rooney, A. Gholinia, K. Watanabe, T. Taniguchi, S. J. Haigh, A. K. Geim, A. I. Tartakovskii, and K. S. Novoselov, *Nature Mat.* **14**, 301 (2014).
- [10] J. S. Ross, S. Wu, H. Yu, N. J. Ghimire, A. M. Jones, G. Aivazian, J. Yan, D. G. Mandrus, D. Xiao, W. Yao, and X. Xu, *Nature Commun.* **4**, 1474 (2013).
- [11] Y. Ye, Z. Ye, M. Gharghi, H. Zhu, M. Zhao, Y. Wang, X. Yin, and X. Zhang, *Appl. Phys. Lett.* **104**, 193503 (2014).
- [12] Z. He, Y. Sheng, Y. Rong, G.-D. Lee, J. Li, and J. H. Warner, *ACS Nano* **9**, 2740 (2015).
- [13] K. L. Seyler, J. R. Schaibley, P. Gong, P. Rivera, A. M. Jones, S. Wu, J. Yan, D. G. Mandrus, W. Yao, and X. Xu, *Nature Nanotech.* **10**, 407 (2015).
- [14] A. Chernikov, A. M. van der Zande, H. M. Hill, A. F. Rigosi, A. Velauthapillai, J. Hone, and T. F. Heinz, *Phys. Rev. Lett.* **115**, 126802 (2015).
- [15] J. Klein, J. Wierzbowski, A. Regler, J. Becker, F. Heimbach, K. Müller, M. Kaniber, and J. J. Finley, *Nano. Lett.* **16**, 1554 (2016).
- [16] J. Kim, X. Hong, C. Jin, S.-F. Shi, C.-Y. S. Chang, M.-H. Chiu, L.-J. Li, and F. Wang, *Science* **346**, 1205 (2014).
- [17] E. J. Sie, J. W. McIver, Y.-H. Lee, L. Fu, J. Kong, and N. Gedik, *Nature Mat.* **14**, 290 (2015).
- [18] G. H. Wannier, *Phys. Rev.* **52**, 191 (1937).
- [19] F. L. Lederman and J. D. Dow, *Phys. Rev. B.* **13**, 1633 (1976).
- [20] A. Chaves, T. Low, P. Avouris, D. Çakır, and F. M. Peeters, *Phys. Rev. B.* **91**, 155311 (2015).
- [21] S. Hastrup, S. Latini, K. Bolotin, and K.S. Thygesen, *Phys. Rev. B.* **94**, 041401 (2016).
- [22] T. G. Pedersen, S. Latini, K. S. Thygesen, H. Mera, and B. K. Nikolic, *New J. Phys.* **18**, 073043 (2016).
- [23] L. V. Keldysh, *JETP Lett.* **29**, 658 (1978).
- [24] P. Cudazzo, I. V. Tokatly, and A. Rubio, *Phys. Rev. B.* **84**, 085406 (2011).
- [25] T. G. Pedersen, H. Mera, and B. K. Nikolić, *Phys. Rev. A.* **93**, 013409 (2016).
- [26] J. Kobus, *Phys. Rev. A.* **91**, 022501 (2015).
- [27] D. W. Kidd, D. K. Zhang, and K. Varga, *Phys. Rev. B.* **93**, 125423 (2015).
- [28] A. Dalgarno and J. T. Lewis, *Proc. R. Soc. Lond. A* **233**, 70 (1955).
- [29] T. G. Pedersen, *Solid State Commun.* **141**, 569 (2007).
- [30] S. Latini, T. Olsen, and K. S. Thygesen, *Phys. Rev. B* **92**, 245123 (2015).
- [31] T. G. Pedersen and T. B. Lyngø, *Phys. Rev. B.* **65**, 085201 (2002).
- [32] J. D. Dow and D. Redfield, *Phys. Rev. B.* **1**, 3358 (1970).
- [33] D. E. Aspnes, *Phys. Rev.* **147**, 554 (1966).
- [34] R. J. Elliott, *Phys. Rev.* **108**, 1384 (1957).
- [35] T. G. Pedersen, P. M. Johansen, and H. C. Pedersen, *Phys. Rev. B.* **61**, 10504 (2000).
- [36] H. A. Mavromatis, *Am. J. Phys.* **59**, 738 (1991).
- [37] M. A. Maize, M. A. Antonacci, and F. Marsiglio, *Am. J. Phys.* **79**, 222 (2011).
- [38] J. Tao, J. W. Chai, Z. Zhang, J. S. Pan, and S. J. Wang, *Appl. Phys. Lett.* **104**, 232110 (2014).